Torres-Castanedo et al., submitted to J. Phys. D: Appl. Phys.

Determination of band offsets of Ga_2O_3:Si/FTO heterojunction for current spreading applications

Carlos G. Torres-Castanedo[1], Kuang-Hui Li[1], Laurentiu Braic[2], Xiaohang Li[1]*

[1] King Abdullah University of Science and Technology (KAUST), Advanced Semiconductor Laboratory, Thuwal 23955-6900, Saudi Arabia

[2] King Abdullah University of Science and Technology (KAUST), Core Labs, Thuwal 23955-6900, Saudi Arabia

**Corresponding author*

KEYWORDS: gallium oxide, FTO, band offset, current spreading layer

ABSTRACT

Because of relatively low electron mobility of Ga_2O_3, it is important to identify proper current spreading materials. Fluorine-doped SnO_2 (FTO) offers superior properties to those of indium tin oxide (ITO) including higher thermal stability, larger bandgap, and lower cost. However, the Ga_2O_3:Si/FTO heterojunction including the important band offset and the I-V characteristics have not been reported. In this work, we have grown the Ga_2O_3:Si/FTO heterojunction and performed X-ray photoelectron spectroscopy (XPS) measurement. The conduction and valence band offsets were determined to be 0.11 and 0.42 eV, indicating a minor barrier for electron transport and a type-I heterojunction. The subsequent I-V measurement of the Ga_2O_3:Si/FTO heterojunction exhibited pseudo-ohmic behavior. The results of this work manifests promising candidacy of FTO for current spreading layers of Ga_2O_3 devices for high temperature and ultraviolet applications.

Ultrawide-bandgap semiconductor gallium oxide (Ga_2O_3) has the potential for superior power and optical devices. Different devices using Ga_2O_3 have been demonstrated such as MOSFETs,[1] MESFETs,[2] FinFETs,[3] and SBDs.[4] Recently, Green et al.[5] reported a Ga_2O_3-based MOSFET with a critical electric field of 3.8 MV/cm, the highest value reported for any transistor. This value is close to half of the theoretical value for Ga_2O_3 (8 MV/cm) but already higher than the theoretical limits for GaN (3 MV/cm) and SiC (3.2 MV/cm).[6] Ga_2O_3 is also suitable for the solar-blind UV photodetector (SBD) due to its large bandgap (4.7-4.9 eV)[7,8,9] and for gas sensors due to its thermal and chemical stability.[10] For instance, Ga_2O_3 thin films have been employed as O_2 sensor at high operating temperatures up to 1000 ºC.[11] Moreover, the availability of conductive Ga_2O_3 substrates makes this material applicable for vertical injection in visible and ultraviolet (UV) III-nitride LED technology.[12,13,14]

Ohmic contacts with low contact resistance are essential to accelerate the development of Ga_2O_3-based devices. Good p-type doping has not been realized for Ga_2O_3[15,16] and thus the discussion of the ohmic contact and the current spreading layer refers to n-type Ga_2O_3 only. Recently, the ohmic behavior of nine different metals on n-type Ga_2O_3 has been studied, showing that In/Au and Ti/Au form ohmic contact after annealing at 600 and 400-500 ºC, respectively.[17,18] However, the ohmic contacts are not sufficient for high performance Ga_2O_3 devices. Because of relatively low electron mobility of Ga_2O_3 (up to 8.2 S cm^{-1}) [19], it is crucial to develop a current spreading layer to reduce current crowding and contact resistance. Recently, Sn-doped indium oxide (ITO) has been studied as a current spreading layer to improve the ohmic contact between metal and Ga_2O_3.[20] The conduction and valence band offsets (CBO and VBO) of the Ga_2O_3/ITO were recently determined to be 0.32 and 0.78 eV by Carey IV *et al.*, respectively.[21] However, ITO is not an ideal candidate for high temperature and UV applications. First, ITO is thermally unstable at high processing or device operation temperatures.[22, 23, 24] Second, the bandgap of ITO is around 4 eV that makes it absorptive for optical applications below 350 nm. On the other hand, fluorine-doped SnO_2 (FTO) could be a better candidate since it is thermally stable even at temperatures higher than 600 ºC.[25] The excellent thermal stability is in particular important for Ga_2O_3–based devices as its thermal conductivity is poor which may cause self-heating effects.[26] Moreover, the bandgap of FTO is moderately larger than that of ITO, as measured in this study and presented below, hereby covering a wider range of spectrum in terms of optical transparency. Furthermore, it is worth mentioning that FTO has lower cost than ITO due to scarcity of indium, which can lower overall device cost.[27]

To explore potentials of FTO as the current spreading layer for n-type Ga_2O_3, it is essential to identify the band alignment of the Ga_2O_3/FTO heterojunction. Ideally, there is no considerable

potential barrier for electron transport at the conduction band edge. Furthermore, a non-rectifying electrical behavior would allow FTO to be employed to complement or replace metal contacts, or serve as the current spreading layer. In this study, we report on the band offset measurement of n-type Ga_2O_3 grown on commercial FTO substrates by X-ray photoelectron spectroscopy (XPS). The crystal structure and optical transmission of the films were studied by X-ray diffraction (XRD) and UV-Vis spectroscopy. The binding energies and core levels of Ga $2p_{3/2}$ and Sn $3d_{5/2}$ were investigated. The valence and conduction band offsets (VBO and CBO) are determined, where a type-I junction was found. In the end, the Ti/Au metal pads were deposited and annealed to measure the I-V curve of the Ga_2O_3:Si/FTO heterojunction. The study paves the way for the use of FTO as the current spreading layer for high temperature and UV applications based on Ga_2O_3.

Ga_2O_3 thin films have been grown by different techniques such as metalorganic chemical vapor deposition (MOCVD),[2,28] molecular beam epitaxy (MBE),[29] hydride vapor phase epitaxy (HVPE),[30] and pulsed laser deposition (PLD)[31] on both native and foreign substrates. The PLD technique with relatively low cost and high versatility has been employed extensively in the Ga_2O_3 research community.[18, 32, 33]. In this study, three samples were prepared (Fig. 1), including a commercial 250 nm thick FTO thin film on glass substrate with a sheet resistance of 6 Ω/square (NANOCS FT15-120-20), and ~350 and ~3 nm thick Ga_2O_3:Si thin films deposited by PLD on two FTO/glass substrates. The number of pulses used for the two depositions was 30,000 pulses and 200 pulses for the 350 and 3 nm thick Ga_2O_3:Si thin films, respectively. The thicknesses were determined by using the growth rate of 0.17 Å/pulse and the number of pulses amid the PLD processes. Prior to PLD, the FTO/glass substrates were sequentially cleaned ultrasonically in acetone and isopropanol, subsequently rinsed in distilled water. Then the 350 and 3 nm Ga_2O_3:Si thin films were deposited under the same condition using a Neocera Pioneer 180 PLD system with a chamber base pressure of less than 1×10^{-7} Torr, equipped with a Coherent 205F laser working at 248 nm. A one-inch Ga_2O_3 target (PVD Products) with 1.6 at% Si was ablated at a repetition rate of 5 Hz and a pulse energy density of 2 J/cm^2. The distance between the target and the substrate was 10 cm. The O_2 pressure was 4.5 mTorr and the substrate temperature was 575 ºC. This temperature is higher than the ITO stability temperature [24,25,26] which enables high temperature deposition of crystallize Ga_2O_3:Si/on commercial FTO.

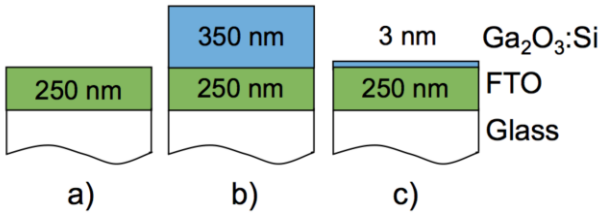

Figure 1 Schematics of the three investigated samples: (a) the commercial FTO/glass substrate, (b) the thick (350 nm) and (c) the thin (3 nm) Ga_2O_3:Si layers deposited on the FTO/glass substrates.

The XPS measurements were carried out immediately after the PLD growth using a Kratos Axis Supra DLD spectrometer with an Al Kα source (λν=1486.6 eV) operating at 150 W without any ex-situ cleaning process. The measured binding energies were referenced to the *C 1s* binding energy of the carbon contamination (284.8 eV) and the step size was set to 0.1 eV for high-resolution XPS acquisition. The binding energy peaks were fitted by the Voigt curve using a Shirley background subtraction[34] in the proximity of the peak, while the valence band maximum (VBM) was calculated by extrapolating the leading edge to zero signal. The crystal structure of the thick Ga_2O_3:Si and the FTO films was examined by a Bruker D8 Advance X-Ray diffractometer with a Cu Kα source (λ=1.5405Å). The optical transmittance of the films was characterized by a Shimadzu UV-3600 spectrophotometer. Ti (20 nm)/Au (80 nm) contacts were deposited on a by DC sputtering at 440 W, followed by a rapid thermal annealing (RTA) treatment at 470 ºC for 60 s in Ar atmosphere performed in a JetFirst 200C system. The I-V curve of the junction was measured by a Keithley 2400 system.

Fig. 2 shows XRD patterns of the 350 nm Ga_2O_3:Si film on the FTO/glass substrate and the FTO/glass substrate itself. These patterns are compared with selected powder peaks of the following JCPDS-ICDD cards: 41-1445 for SnO_2 tetragonal-rutile and 43-1012 for Ga_2O_3 monoclinic. The FTO/glass substrate contains (101), (110), (200), (211), and (220) planes. As a result, it is expected the grown Ga_2O_3:Si film to follow some of those planes regardless of the growth or epitaxy techniques. The deposited Ga_2O_3:Si film presents a monoclinic structure (β) with two main orientations, predominantly (110) with (400) at much lower intensity (Inset of Fig. 2). These growth directions are consistent with the intensity of (110) and (200) peaks of the FTO film, indicating that Ga_2O_3 grew following mainly the (110) plane and marginally the (200) plane of FTO. Due to the monoclinic crystal structure of Ga_2O_3, the film did not grow in the direction of any of the other three planes, i.e. (101), (211), and (220) of the FTO/glass substrate.

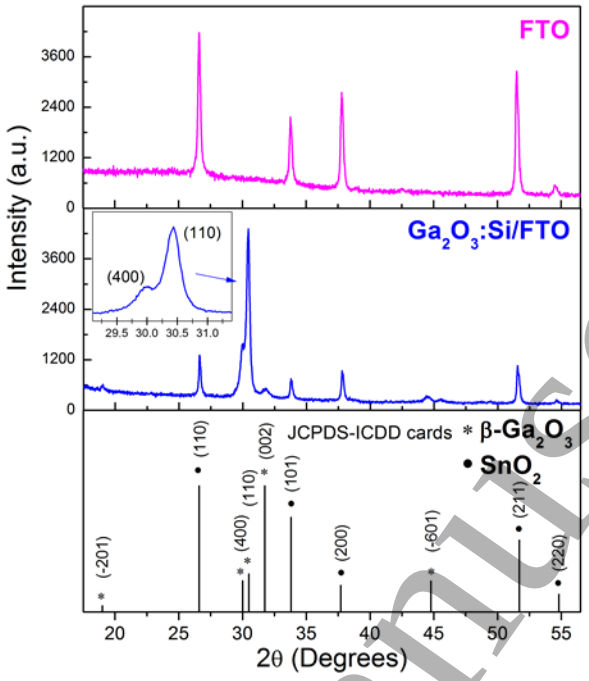

Figure 2 XRD patterns of the FTO/glass substrate and the 350 nm Ga_2O_3:Si film deposited on the FTO/glass substrate. The inset shows the two preferred monoclinic directions for Ga_2O_3:Si film in (110) and (400). The patterns are compared to JCPDS-ICDD cards 41-1445 (SnO_2) and 43-1012 (Ga_2O_3).

To facilitate the determination of the band offsets, the bandgap (E_g) of Ga_2O_3:Si and FTO were firstly deduced from transmission spectra. Since E_g of Ga_2O_3 is larger than that of FTO, it is not possible to measure it on the FTO/glass substrate. Thus, another 350 nm Ga_2O_3:Si layer was grown under the same conditions as the Ga_2O_3 (350 nm)/FTO/glass sample on the optically transparent *c*-sapphire substrate. Fig. 3 shows the transmission measurement for both films using the air baseline while the inset displays the Tauc plot[35] ($h\nu$ *vs.* $(\alpha h\nu)^n$) in which n=2 was used for directly allowed transitions. The calculated E_g's are 4.94±0.01 eV and 4.40±0.02 eV for Ga_2O_3:Si and FTO, respectively. In the case of Ga_2O_3:Si, an increment of E_g compared to undoped Ga_2O_3 (E_g=4.7-4.9eV)[9,10] has been observed concomitantly with the increase of Si content in the film.[36] The E_g of FTO is higher than some reported values (~4.10 eV)[37,38] but it agrees well with the transmission spectra from NANOCS which supplied the FTO substrates for this study.[39]

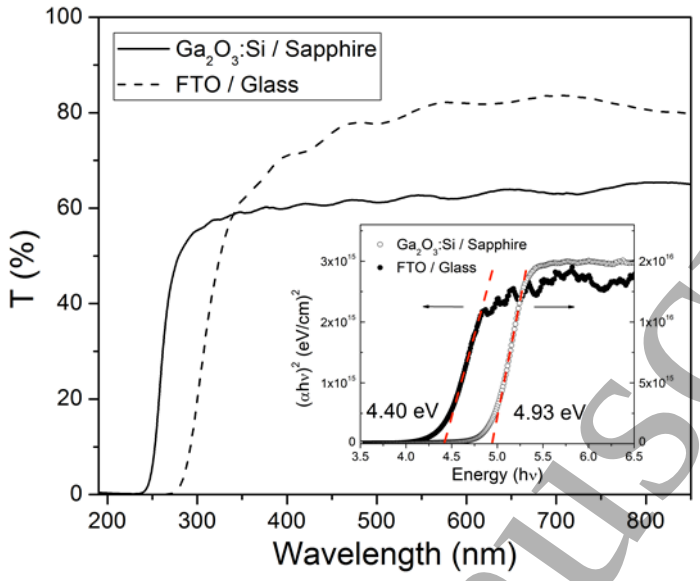

Figure 3 Transmission spectra of the 350-nm thick Ga_2O_3:Si thin films deposited on sapphire and FTO/glass substrates. Inset shows the Tauc plot $h\upsilon$ vs. $(\alpha h\upsilon)^2$ with the E_g values for each film.

To determine the band offsets at the heterojunction interface, the Kraut's method[40] was utilized to analyze the XPS spectra of the three samples shown in Fig. 1. First, the core level binding energies and the VBM of the FTO and the 350 nm Ga_2O_3:Si layer were determined. The 3 nm Ga_2O_3:Si on FTO was measured for the binding energy difference between the two reference core levels at the interface. In all the peak fittings, the Shirley background and Voigt curves were employed. Fig. 4 shows the XPS results. The selected core levels are *Ga 2p*$_{3/2}$ and *Sn 3d*$_{5/2}$ since these are the most intense peaks observed in the XPS survey spectra. The calculation of the VBM for both the Ga_2O_3:Si/FTO and FTO is shown in the insets of Fig. 4 a and b, respectively. One Voigt curve allowed the proper fitting of the *Ga 2p*$_{3/2}$ binding energy of both the thick as well as the thin Ga_2O_3:Si film on FTO (Fig. 4 a and c). On the other hand, the *Sn 3d*$_{5/2}$ peak is not symmetric due to the contribution of Sn^{4+} and Sn^{2+} (Fig. 4 b and c).[41,42] Table 1 summarizes the core levels and VBM values of the samples.

Equations 1 and 2 are used to calculate the valence band offset (VBO) and the conduction band offset (CBO), respectively.[11] The sequence of the terms in parenthesis in Eq. 1 corresponds to the XPS results in Fig. 4 a), b), and c. In order to calculate the CBO (Eq. 2), the difference between the E_g of Ga_2O_3:Si and FTO films was used.

$$\Delta E_V = \left(E_{Ga\ 2p}^{Ga_2O_3} - E_{VBM}^{Ga_2O_3}\right) - \left(E_{Sn\ 3d}^{FTO} - E_{VBM}^{FTO}\right) - \left(E_{Ga\ 2p}^{Ga_2O_3} - E_{Sn\ 3d}^{FTO}\right), \textit{Eq. 1}$$

$$\Delta E_C = \left(E_g^{Ga_2O_3} - E_g^{FTO}\right) - \Delta E_V, \textit{Eq. 2}$$

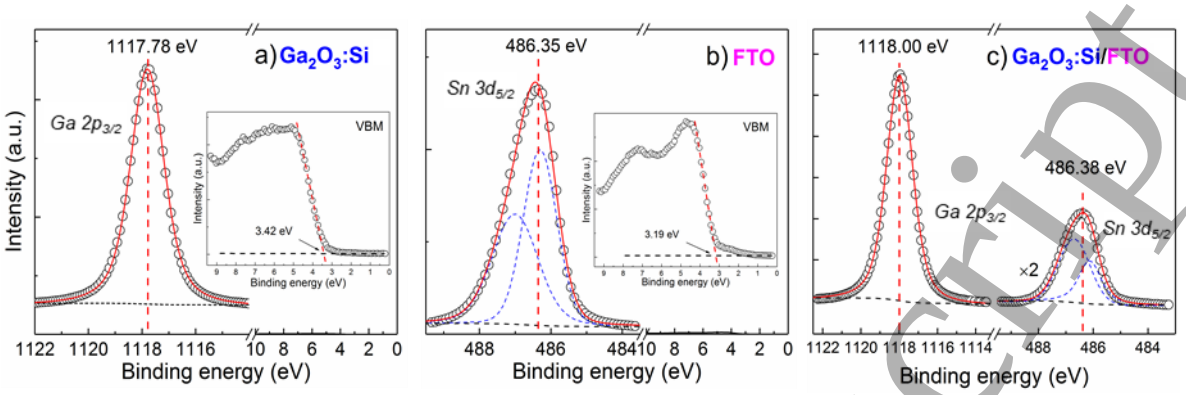

Figure 4 Core level *Ga 2p*$_{3/2}$ and VBM spectra of the ~350 nm Ga_2O_3:Si on FTO (a). Core level *Sn 3d*$_{5/2}$ and VBM spectra of the 250 nm FTO (b). Core level *Ga 2p*$_{3/2}$ and $Sn3d_{5/2}$ of the 3 nm Ga_2O_3: Si on FTO (c). The core levels were fitted by Voigt curves, and using the Shirley background.

Table 1 Peak positions of core levels and VBM used to calculate the band offset in the Ga_2O_3:Si/FTO junction.

Sample	Region	Binding energy (eV)
Ga_2O_3:Si	*Ga 2p*$_{3/2}$ VBM	1117.78 3.42
FTO	*Sn 3d*$_{5/2}$ VBM	486.35 3.19
Ga_2O_3:Si / FTO	*Ga 2p*$_{3/2}$ *Sn 3d*$_{5/2}$	1118.00 486.38

The diagram in Fig. 5a shows the band alignment diagram of the heterojunction. It shows that the Ga_2O_3:Si/FTO junction has a straddling-gap (type-I) alignment, with VBO ΔE_V of 0.42 eV and CBO ΔE_C of 0.11 eV. Since the ΔE_C is small, this alignment is desirable for electron transport across the heterointerface. Previously, a type-I junction was reported for Ga_2O_3 deposited by PLD on the (111) Si substrate with ΔE_C as low as 0.2 eV.[43] In another study, the band offset of ITO/Ga_2O_3 was ΔE_C = 0.32 eV and a type-I junction.[23] Our results show twice and three times lower ΔE_C than these two studies, respectively, which favor the electron transport. There might be strain in the Ga_2O_3 layer due to lattice mismatch. However, previous works have shown that the impact of strain on CBO and VBO is nearly negligible by comparing the unstrained and strained heterojunctions.[44,45]

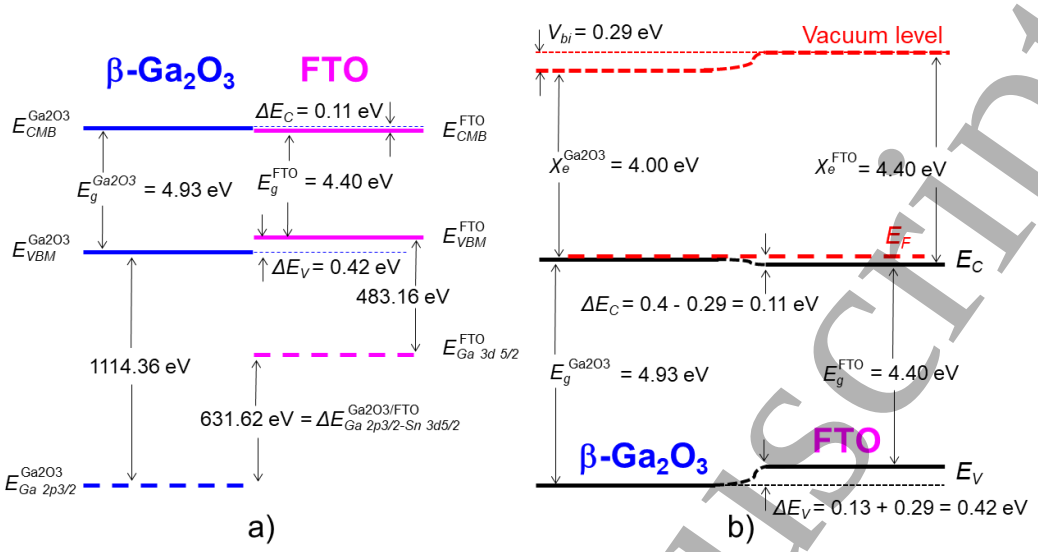

Figure 5 (a) Band alignment diagram for the Ga_2O_3/FTO heterojunction obtained by XPS and (b) the band diagram schematic with the band bending in the junction.

Furthermore, the band bending for the Ga_2O_3:Si/FTO heterojunction is shown in Figure 5b, aligning the Fermi level of both materials. The effective density of states function in the conduction band for both materials was calculated considering an effective electron mass (m_n^*) of 0.28 m_o corresponding to SnO_2 and Ga_2O_3.[46,47] According to our Hall effect measurements at room temperature, the concentrations of electrons were 9.1×10^{20} and 1.0×10^{19} cm^{-3} for FTO and Ga_2O_3:Si films, respectively. This measurement was done using an Ecopia HMS-3000 Hall system with a 1 T magnet and following the van der Pauw method. Hence, the Fermi levels for the materials are located above the conduction band (0.14 eV for FTO and 0.03 eV for Ga_2O_3). Considering the calculated Fermi levels and the reported electron affinities (χ_e) for Ga_2O_3 (4.0 eV) and FTO (4.4 eV) [48,49], a built-in potential (V_{bi}) of 0.29 eV was obtained. A type-I junction is still observed with the same ΔE_V and ΔE_C compared to the band alignment study due to band bending. It is important to note that this treatment does not consider interface states. To investigate the electrical properties of the Ga_2O_3/FTO and FTO/metal heterojunctions, we performed I-V measurement at room temperature. Two sets of metallic masks were used, first to deposit the Ga_2O_3:Si thin film on the FTO/glass substrate and second to deposit two sets of 1×10 mm^2 Ti (20 nm)/Au (80 nm) contacts on the Ga_2O_3:Si thin film. The I-V curve and the schematic are presented in Fig. 6. The I-V curve was measured before and after rapid thermal annealing (RTA) of the complete measured heterostructure at 470 ºC in Ar atmosphere to improve the quality of the Ti/Au contacts. After annealing, the resistance decreased significantly from approximately 27 to 12 Ω while the ohmic behavior was improved in the ±1 V, indicating that FTO can be an encouraging current spreading layer for Ga_2O_3.

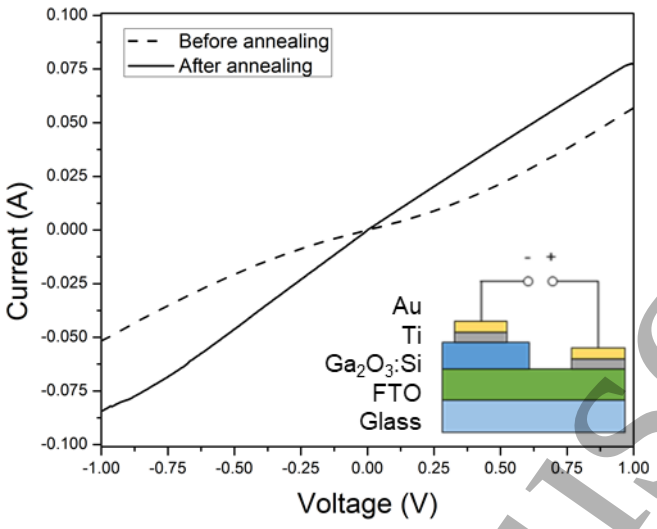

Figure 6 I-V curves of the Ga_2O_3:Si/FTO junction before and after the annealing process for the Ti/Au contacts. Inset shows the cross-sectional schematics.

In summary, we reported on formation and characterization of the Ga_2O_3:Si//FTO heterojunction. In particular, we have performed high-resolution XPS measurements to determine that Ga_2O_3:Si/FTO heterojunction has a straddling-gap (type-I) alignment with ΔE_V of 0.42 eV and ΔE_C of 0.11 eV. The junction exhibits a pseudo-ohmic behavior with Ti/Au contacts after annealing. The small $\underline{\Delta E_C}$ and the non-rectifying behavior of the junction, as well as the large $\underline{E_g}$ of 4.40 eV and reported thermal stability at high temperature,[22,23,24] make FTO a promising candidate for use as a current spreading layer in Ga_2O_3-based high temperature and short wavelength devices.

The authors would like to acknowledge the support of KAUST Baseline BAS/1/1664-01-01, KAUST Competitive Research Grant URF/1/3437-01-01 and URF/1/3771-01-01, and GCC Research Council REP/1/3189-01-01.

References

[1] M. H. Wong, K. Sasaki, A. Kuramata, S. Yamakoshi, and M. Higashiwaki, IEEE Electron Device Lett. **37**, 212 (2016).

[2] M. Higashiwaki, K. Sasaki, A. Kuramata, T. Masui, and S. Yamakoshi, Appl. Phys. Lett. **100**, 013504 (2012).

[3] K. D. Chabak, N. Moser, A. J. Green, D. E. Walker Jr., S. E. Tetlak, E. Heller, A. Crespo, R. Fitch, J. P. McCandless, K. Leedy, M. Baldini, G. Wagner, Z. Galazka, X. Li, and G. Jessen, Appl. Phys. Lett. **109**, 213501 (2016).

[4] M. Higashiwaki, K. Konishi, K. Sasaki, K. Goto, K. Nomura, Q. T. Thieu, R. Togashi, H. Murakami, Y. Kumagai, B. Monemar, A. Koukitu, A. Kuramata, and S. Yamakoshi, Appl. Phys. Lett. **108**, 133503 (2016).

[5] A. J. Green, K. D. Chabak, E. R. Heller, R. C. Fitch, M. Baldini, A. Fiedler, K. Irmscher, G. Wagner, Z. Galazka, S. E. Tetlak, A. Crespo, K. Leedy, and G. H. Jessen, IEEE Electron Device Lett. **37**, 902 (2016).

[6] M. A. Mastro, A. Kuramata, J. Calkins, J. Kim, F. Ren, and S. J. Pearton, ECS J. Solid State Sci. Technol. **6**, 356 (2017).

[7] F. -P. Yu, S. -L. Ou, D. -S. Wuu, Opt. Mater. Express **5**, 1240 (2015).

[8] M. Higashiwaki, K. Sasaki, A. Kuramata, T. Masui, and S. Yamakoshi, Phys Status Solidi A **211**, 21 (2014).

[9] D. Y. Guo, Z. P. Wu, Y. H. An, X. C. Guo, X. L. Chu, C. L. Sun, L. H. Li, P. G. Li, and W. H. Tang, Appl. Phys. Lett. **105**, 023507 (2014).

[10] M. Ogita, K. Higo, Y. Nakanishi, and Y. Hatanaka, Appl. Surf. Sci. **721**, 175 (2001).

[11] M. Bartic, C. -I. Baban, H. Suzuki, M. Ogita, and M. Isaki, J. Am. Ceram. Soc. **90**, 2879 (2007).

[12] H. Liu, V. Avrutin, N. Izyumskaya, Ü. Özgür, and H. Morkoç, Superlattices Microstruct. **48**, 458 (2010).

[13] M. M. Muhammed, M. A. Roldan, Y. Yamashita, S. -L. Sahonta, I. A. Ajia, K. Iizuka, A. Kuramata, C. J. Humphreys, and I. S. Roqan, Sci. Rep. **6**, 29747 (2016).

[14] M. M. Muhammed, N. Alwadai, S. Lopatin, A. Kuramata, and I. S. Roqan, ACS Appl. Mater. Interfaces **9**, 34057 (2017).

[15] A. Kyrtsos, M. Matsubara, and E. Belloti, Appl. Phys. Lett. **112**, 032108 (2018).

[16] E. Chikoidze, A. Fellous, A. Perez-Tomas, G. Sauthier, T. Tchelidze, C. Ton-That, T. T. Huynh, M. Phillips, S. Russell, M. Jennings, B. Berini, F. Jomard, and Y. Dumont, Mater. Today Phys. **3**, 118 (2017).

[17] Y. Yao, R. F. Davis, and L. M. Porter, J. Electron. Mater. **46**, 2053 (2017).

[18] M. Higashiwaki, K. Sasaki, H. Murakami, Y. Kumagai, A. Koukitu, A. Kuramata, T. Masui, and S. Yamakoshi, Semicond. Sci. Technol. **31**, 034001 (2016).

[19] M. Orita, H. Hiramatsu, H. Ohta, M. Hirano, and H. Hosono, Thin Solid Films, **411** 134 (2002).

[20] T. Oshima, R. Wakabayashi, M. Hattori, A. Hashiguchi, N. Kawano, K. Saskai, T. Matsui, A. Kuramata, S. Yamakoshi, K. Yoshimatsu, A. Ohmoto, T. Oishi, and M. Kasu, Jpn. J. Appl. Phys. **55**, 1202B7 (2016).

[21] P. H. Carey, IV, F. Ren, D. C. Hays, B. P. Gila, S. J. Pearton, S. Jang, and A. Kuramata, Appl. Surf. Sci. **422**, 179 (2017).

[22] T. Minami, T. Miyata, and T. Yamamoto, J. Vac. Sci. Technol. A **17**, 1822 (1999).

[23] W. -J. Choi, D. -J. Kwak, C. -S. Park, Y., and -M. Sung, J. Nanosci. Nanotechnol **12**, 3394 (2012).

[24] C. M. Chen, T. -C. Hsu, and S. -J. Cherng, J. Alloys Compd. **509**, 872 (2011).

[25] D.-J.Kwak, B. -H, Moon, D. -K. Lee, C. -S., Park, and Y. -M. Sung, J. Electr. Eng. Technol. **6**, 684 (2011).

[26] S. I. Stepanov, V. I. Nikolaev, V. E. Bougrov, and A. E. Romanov, Rev. Adv. Mater. Sci. **44**, 63 (2016).

[27] T. Minami and T. Miyata, Thin Solid Films **517**, 1474 (2008).

[28] D. Gogova, G. Wagner, M. Baldini, M. Schmidbauer, K. Irmscher, R. Schewski, Z. Galazka, M. Albrecht, and R. Fornari, J. Cryst. Growth **401**, 665 (2014).

[29] K. Sasaki, M. Higashiwaki, A. Kuramata, T. Masui, and S. Yamakoshi, J. Cryst. Growth **378**, 591 (2013).

[30] H. Murakami, K. Nomura, K. Goto, K. Sasaki, K. Kawara, Q.T. Thieu, R. Togashi, Y. Kumagai, M. Higashiwaki, A. Kuramata, S. Yamakoshi, B. Monemar, and A. Koukitu, Appl. Phys. Express **8**, 015503 (2015).

[31] K. D. Leedy, K. D. Chabak, V. Vasilyev, D. C. Look, J. J. Boeckl, J. L. Brown, S. E. Tetlak, A. J. Green, N. A. Moser, A. Crespo, D. B. Thomson, R. C. Fitch, J. P. McCandless, and G. H. Jessen, Appl. Phys. Lett. **111**, 012103 (2017).

[32] S. Müller, H. von Wenckstern, D. Splith, F. Schmidt, and M. Grundmann, Phys. Status Solidi A **211**, 34 (2014).

[33] F. Zhang, K. Saito, T. Tanaka, M. Nishio, and Q. X. Guo, J. Mater. Sci.: Mater. Electron. **26**, 9624 (2015).

[34] D.A. Shirley, Phys. Rev. **55**, 4709 (1972).

[35] J. Tauc, R. Grigorovici, and A. Vancu, Phys. Status Solidi (b) **15**, 627 (1966).

[36] K. Takakura, D. Koga, H. Ohyama, J.M. Rafi, Y. Kayamoto, M. Shibuya, H. Yamamoto, and J. Vanhellemont, Physica B **404**, 4854 (2009).

[37] B. Stjerna, E. Olsson, and C.G. Granqvist, J. Appl. Phys. **76**, 3797 (1994).

[38] A. E. Rakhshani, Y. Makdisi, and H. A. Ramazaniyan, J. Appl. Phys. **83**, 1049 (1998).

[39] NANOCS, FTO Coated Glass Slides 25x75x2 mm. http://www.nanocs.net/FTO-glass-5ohm-20.htm, 2018 (accessed 26 May 2018).

[40] E. A. Kraut, R. W. Grant, J. R. Wladrop, and S. P. Kowalczyk, Phys. Rev. Lett. **44**, 1620 (1980).

[41] J. K. Yang, H. L. Zhao, and F. C. Zhang, Mater. Lett. **90**, 37 (2013).

[42] T. Li, X. Zhang, J. Ni, J. Fang, D. Zhang, J. Sun, C. Wei, S. Xu, G. Wang, and Y. Zhao, Sol. Energy **134**, 375 (2016).

[43] Z. Chen, K. Nishihagi, X. Wang, K. Saito, T. Tanaka, M. Nishio, M. Arita, and Q. Guo, Appl. Phys. Lett. **109**, 102106 (2016).

[44] C. G. Van de Walle and J. Neugebauer, Appl. Phys. Lett. **70**, 2577 (1997).

[45] S. Wei and A. Zunger, Appl. Phys. Lett. **69**, 2719 (1996).

[46] K. J. Button, C. G. Fonstad, and W. Dreybrodt, Phys. Rev. B **4**, 4539 (1971).

[47] C. Janowitz, V. Scherer, M. Mohamed, A. Krapf, H. Dwelk, R. Manzke, Z. Galazka, R. Uecker, K. Irmscher, and R. Fornari, New J. Phys. **13**, 085014 (2011).

[48] M. Mohamed, K. Irmscher, C. Janowitz, Z. Galazka, R. Manzke, and R. Fornari, App. Phys. Lett. **101**, 132106 (2012).

[49] M. G. Helander, Z. Greiner, Z. B. Wang, and W. M. Tang, J. Vac. Sci. Technol. A **29**, 011019 (2011).